Noname manuscript No.
(will be inserted by the editor)

Amplitude hysteresis and the synchronization region

Prediction of vortex-induced vibration using a freely forced van der Pol oscillator

Øyvind Mortveit Ellingsen · Xavier Amandolese

Received: date / Accepted: date

Abstract Vortex-induced vibration is a nonlinear phenomenon that can damage buildings or produce energy. Here, the range of synchronization between fluid and structure is an important parameter. Using a coupled van der Pol and linear oscillator system, we derived an analytic, closed-form expression for the synchronization range as a function of fluid shedding frequency, or lock-in as it's also called. Our new definition is an improvement to an earlier synchronization definition as it includes the effect of dissipation; without it hysteresis is missing. The fluid speed range with hysteresis is found to be non-monotonic with forcing strength while the region of absolute synchronization increases monotonically. Our proposed synchronization definition can be a useful tool when designing structural dampers or energy harvesters but is a general solution for all systems that can be modeled with similarly coupled equations.

Keywords Synchronization · Vortex-induced vibrations · Hysteresis · van der Pol oscillator

1 Introduction

Interesting behaviors can be observed in systems consisting of a van der Pol coupled with a linear oscillator. If correctly coupled, the system exhibit absolute and conditional synchronization, i.e. amplitude hysteresis. Synchronization conditions are defined for harmonically forced van der Pol oscillators with weak nonlinearity [1] but a literature review has not given results for our system. We'll therefore define it for "freely" forced van der Pol oscillator. The wording "freely" forced comes from the linear oscillator acting like a harmonic force with amplitude and frequency dependent on the van der Pol oscillator it forces. This weakly nonlinear system can have steady solutions but is chaotic when the nonlinearity is strong [7].

Bishop and Hasan observed that vortex-induced vibrations [4] have similar characteristics as the coupled system investigated; the synchronization is referred to as "lock-in" in this field. Their experiment showed that a cylinder oscillating perpendicular to the flow experiences synchronization, amplitude hysteresis and a nonlinear, self-excited force due to periodic vortex shedding. Similar behavior have been successfully modeled using Rayleigh and van der Pol oscillators [11].

Based on these works, and a wake model by Birkhoff and Zarantonello [3], Facchinetti, de Langre and Biolly [6] devised a simple model coupling the oscillating force with a linear structural oscillator. In the structural model, a force following the motion of a scaled wake is used. This wake is modeled using a weakly nonlinear van der Pol oscillator with a forcing term proportional to structural acceleration. This means that both the wake motion (or aerodynamic lift force) and structural motion drive each other.

Meliga and Chomaz validated the wake coupling [10] with an asymptotic flow analysis of the Navier-Stokes equations at low Reynolds numbers. They showed that an elastically mounted cylinder affected the fluid forcing with terms proportional to structural acceleration

Ø. M. Ellingsen
CAPE, CSTB, 44300, Nantes, France and
LadHyX, École polytechnique-CNRS, 91128, Palaiseau, France.
E-mail: oyvind@ladhyx.polytechnique.fr
ORCID iD: 0000-0001-7720-6670

X. Amandolese
LMSSC, CNAM, 75003, Paris, France and
LadHyX, École polytechnique-CNRS, 91128, Palaiseau, France.
E-mail: xavier.amandolese@lecnam.net

and a negligible structural jerk or integral term. The extra term was suggested to improve the model but exact parameter values were neglected. Facchinetti et al. weren't the first researchers to use this coupling term. Tamura and Matsui [12] used both structural acceleration and dissipation in their Birkhoff-based and more complex wake-oscillator model.

Vortex-induced vibration can damage civil engineering structures or be used to extract energy. Barrero-Gil, Pindado and Avila [2] postulated that dimensionless mass governs the fluid velocity range of efficient energy extraction; this being the the lock-in region. Dai, Abdelkefi and Wang's result corroborate the importance of synchronization in producing power when using a beam connected to a circular cylinder exposed to uniform flow [5]. Their numerical results show that combining vortex-induced vibration with steady base excitation increases the produced power by 150 % compared with base excitation only.

Xia, Michelin and Doaré [13] found that a flapping flag experiences similar synchronization and efficiency behavior. They further indicate that synchronization is expected in many fluid-structure interaction systems. This shows that a coupled linear and van der Pol oscillator system can be used to model more than vortex-induced vibrations.

The lock-in limits for vortex-induced vibration has been studied and estimated. de Langre [9] derived an analytic expression using the model of Facchinetti et al. where all dissipation terms were neglected. When evaluating the stability of the now linear system, de Langre concluded that lock-in was due to coupled-mode flutter. Zhang, Li, Ye and Jiang [14] verified the "flutter-induced lock-in" using a coupled FEM and CFD code, but found that the synchronization first starts as resonance before transitioning to flutter.

Unsatisfied with the synchronization limits of de Langre, we'll develop a different analytic definition. The new definition has the same basis but includes the nonlinear and dissipation terms. The proposed definition is a general solution for a van der Pol oscillator coupled to a linear oscillator with both dissipation and reactive coupling terms. A priori knowledge of the synchronization regions allows us to easily find when we can have multiple solutions and estimate the fluid speeds that causes excessive movements or the highest energy harvesting efficiency.

This paper is organized as follows. First the model and approximation is described. Then an analytic expression for the synchronization regions is derived and how it changes with forcing strength and damping is explored. We'll finish with a discussion on the uses and usefulness of our results before concluding.

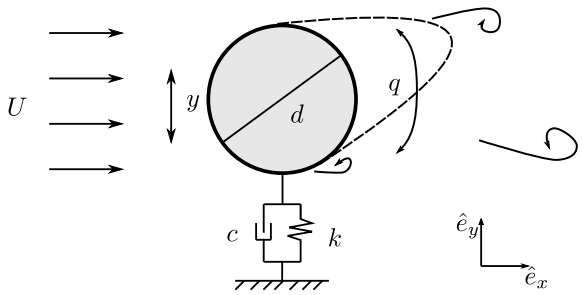

Fig. 1 Simplified sketch of the coupled fluid-structure interaction system used to model the vortex-induced vibration of a cylinder exposed to a uniform free-stream.

2 The vortex-induced vibration model

2.1 Model description

Figure 1 shows a simplified sketch of the system. The structure is limited to oscillation in the $\hat{e}_y$ direction and the wake oscillates behind the cylinder due to the periodic shedding of vortexes. This structural motion has two effects on the total dynamics: It induces a mass-scaled drag force ($\gamma\omega_q\mu^{-1}\hat{e}_y$) on the structure and changes the wake motion. Diameter (d), structural stiffness (k) damping c, fluid density ρ and dimensionless shedding frequency (the Strouhal number St) are assumed to be constant and incoming fluid speed (U) to be steady. The structural mass per unit length (m) is postulated to affect the synchronization region and is the main structural variable. Defining a new dimensionless shedding frequency as $\omega_q = StU(2\pi\omega_n d)^{-1}$, where ω_n is the natural structural frequency, simplifies notation and makes the wake frequency clearer.

The vortex-induced vibration is modeled using the coupled wake-oscillator model of Facchinetti et al. [6]; this is a simple model with a linearly defined synchronization region [9]. The model couples structural motion with a mass-scaled lift force ($M = F\mu^{-1}$) that's amplified and oscillates based the wake motion. It is described in equation 1 with total damping $D(\omega_q)$ given in equation 3. This wake motion, described in equation 2, is modeled as a weakly nonlinear van der Pol oscillator forced by the acceleration of the structure. The equations can be written as

$$\ddot{y} + D(\omega_q)\dot{y} + y = \omega_q^2 M q, \tag{1}$$

$$\ddot{q} + \epsilon\left(q^2 - 1\right)\dot{q} + \omega_q^2 q = A\ddot{y}, \tag{2}$$

$$D(\omega_q) = 2\zeta + \frac{\gamma}{\mu}\omega_q, \tag{3}$$

when dimensionless time is defined using ω_n ($\tau = t\omega_n$).

This system is simpler to process if we rewrite it. Using equation 1, the structural acceleration term in equation 2 can be substituted. The new equation shows

that acceleration coupling is a combination of both dissipative and reactive coupling plus a modification of the linear wake frequency ω_q as shown in equation 4 below

$$\ddot{q} + \epsilon\left(q^2 - 1\right)\dot{q} + \omega_q^2(1 - AM)q = -AD(\omega_q)\dot{y} - Ay. \quad (4)$$

So far, the fluid dynamic terms haven't been defined. An exact definition isn't necessary when seeking a general solution for the synchronization regions of similar systems. Our dimensionless parameters are defined as

$$\mu = \frac{m + 0.25\pi\rho d^2 C_m}{\rho d^2}, \quad (5)$$

$$\gamma = \frac{5}{3}\frac{C_D}{4\pi St}, \quad (6)$$

$$F = \frac{C_{Lo}}{16\pi^2 St^2}. \quad (7)$$

where γ and F are aerodynamic parameters treated as constants in our analysis and μ is variable. μ is a mass-ratio that scales both the added drag (γ) and lift (F) force and are given in equations 5, 6 and 7 respectively. The coefficients C_m, C_D and C_{Lo} are respectively the added mass, mean drag and unsteady lift coefficient for a fixed structure.

Now that the model and its parameters are defined, steady-state amplitudes of wake and structural motion and their phase difference can be approximated.

2.2 Model approximation

Numerically solving the equations of motion for all parameter combinations and in the shedding frequency range of interest ($\omega_q \in [0.5, 3.5]$) is time consuming, some might say a pain in the butt. At the end of the day, it may give little to no insight into how the oscillation amplitude vary with a given parameter. What we want, is some simpler equations that estimates the phase difference between structural and wake motion as well as their amplitudes.

To this end, the Krylov-Bogoliubov method of averaging, as described by Balanov et al. [1], is used. For those unfamiliar with the approximation, here is a short introduction. First, assume that the solution to a nonlinear differential equation is a quasi-harmonic function in time with time varying phase lag and amplitude ($x = r_x\cos(\omega t + \phi_x(t))$) and impose a condition on the time derivative of amplitude and phase terms. Insert this condition and assumed solutions into the nonlinear differential equation and average everything over one period of a fast oscillation. Fast is the keyword, and the oscillations are assumed to be much faster than the change in both amplitude and phase over one cycle of oscillation. Equations describing the time derivative of amplitudes and phase lags are recovered by separating the averaged equations by real and imaginary parts. Using the individual phase lags, phase difference between two equations can be defined.

Using the mentioned technique, equations 1 and 4 are approximated to the following set of equations:

$$\dot{r}_y = \frac{1}{2}\left(\frac{\omega_q^2}{\omega}Mr_q\sin(\theta) - Dr_y\right), \quad (8)$$

$$\dot{r}_q = \frac{\epsilon\omega_q}{2}\left(r_q - \frac{r_q^3}{4}\right) + \frac{Ar_y}{2}\left(\frac{\sin(\theta)}{\omega} - D\cos(\theta)\right), \quad (9)$$

$$\dot{\theta} = \frac{\omega_q^2(1 - AM) - 1}{2\omega} + \frac{ADr_y}{2r_q}\sin(\theta) + \left(\frac{\omega_q^2 Mr_q}{2\omega r_y} + \frac{Ar_y}{2\omega r_q}\right)\cos(\theta), \quad (10)$$

where $D(\omega_q)$ has been shortened to D and phase difference $\theta = \phi_q - \phi_y$ replaces individual phase lags. Equations 8–10 requires some more work to be fully useful for us; we'll solve them at steady state and eliminate the time derivative terms. Rewriting the r_y outside equation 8 and all $\frac{r_y}{r_q}$ terms gives

$$r_y = \frac{\omega_q^2 M}{\omega D}r_q\sin(\theta), \quad (11)$$

$$r_q = 2\left[1 + \frac{\omega_q AM\sin(\theta)}{\epsilon\omega D}\left(\sin(\theta) - D\cos(\theta)\right)\right]^{0.5}, \quad (12)$$

$$0 = \frac{\omega_q^2(1 - AM) - 1}{\omega} + \frac{\omega_q^2 AM}{\omega}\sin^2(\theta) + \left(\frac{D}{\sin(\theta)} + \frac{\omega_q^2 AM}{\omega^2 D}\sin(\theta)\right)\cos(\theta). \quad (13)$$

Equations 11 and 12, structural and wake amplitude respectively, are easy to solve provided that you have solved for the phase differences in quation 13. It may look difficult to solve, but analytic closed-form solutions for θ exist. Using algebra and trigonometric identities, equation 13 can be rewritten as the cubic equation system (with $x = sin^2(\theta)$) defined in equations 14–18.

$$0 = ax^3 + bx^2 + cx + d, \quad (14)$$

$$a = \omega_q^4 A^2 M^2\left[1 + (\omega D)^{-2}\right], \quad (15)$$

$$b = 2\omega_q^2 AM\left[\omega_q^2(1 - AM) - 1\right] + 2\omega\omega_q^2 AM - \frac{\omega_q^4 A^2 M^2}{\omega^2 D^2}, \quad (16)$$

$$c = \left[\omega_q^2(1 - AM) - 1\right]^2 - 2\omega_q^2 AM + \omega^2 D^2, \quad (17)$$

$$d = -\omega^2 D^2. \quad (18)$$

The solutions for $\sin^2(\theta)$ are found using a general cubic formula and only the non-complex solutions are kept; all complex solutions are dismissed as nonphysical. Of the possible θ solutions, we have limited us to

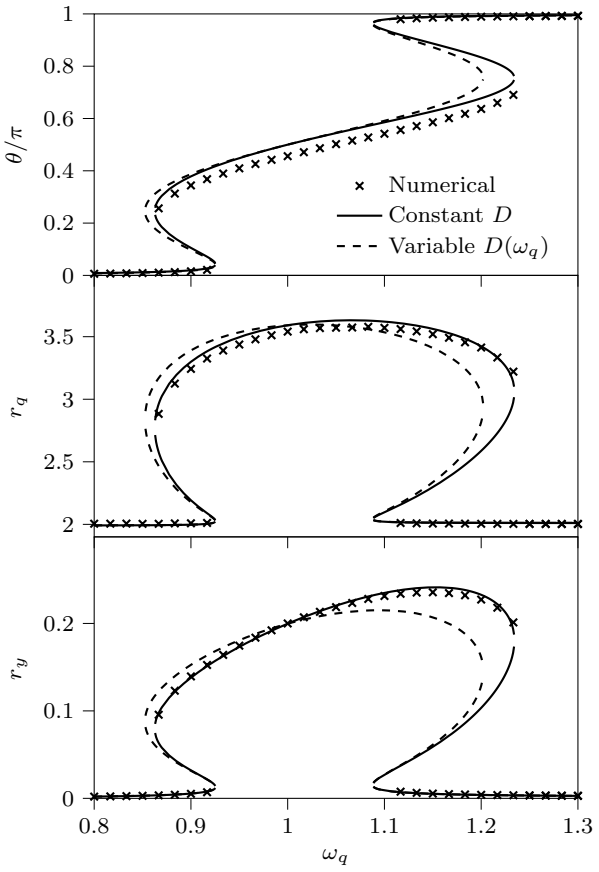

Fig. 2 Validation of approximation and choice of $D(\omega_q)$. Top graph shows the phase difference, middle the wake amplitude and bottom the structural amplitude.

$\theta \in [0, \pi]$ and enforce that $\theta > \pi/2$ for $\omega_q > 1$. This ensures that structural amplitude is positively defined and that $\theta(\omega_q)$ is smooth for all solution branches.

With the amplitudes and phase difference approximations expressed in closed-form analytic form, the hysteresis regions and a definition of synchronization regions can be found. Before this, we need to validate that the approximation is correct and determine better values for the parameters used in equations 14–18.

2.3 Validation of the approximation

The approximation has given some nice expressions for phase difference and amplitudes, but these are meaningless if they don't mimic reality (or in this case, the numerical simulations). For the numerical simulations, the amplitudes are found by finding the mean amplitudes from long numerical simulations at each ω_q. The phase difference θ is defined as the phase difference between fast Fourier transforms of the wake and structural time signals at the dominant structural frequency (either ω_q or ω_n). Before attempting a validation, the

Table 1 Parameters used in the validation and for synchronization region plots.

Parameter	Value
ϵ	0.3
A	12
C_m	1
γ	0.442
F	0.0401
ζ	0.00191
μ	72.9

forcing frequency ω in the approximation need to be determined. Two values comes to mind: the dimensionless natural structural frequency and the dimensionless shedding frequency (i.e. $\omega = 1$ or $\omega = \omega_q$).

To decide the value of ω, let's do some deduction. There are two characteristic frequencies in the system: the natural structural frequency and the linear natural frequency of the van der Pol oscillator. The structural frequency is kept constant and the van der Pol frequency varies linearly with fluid speed. Strong structural motion only affects the wake amplitude and shedding frequency when the wake frequency is close to the structural one. If the wake equation was a forced van der Pol oscillator (i.e. prescribed motion), the forcing frequency would be the frequency of structural motion. In the case of free vibration, this would be the natural structural frequency. Based on these postulates, we feel it is justified to set ω as the structural frequency. I.e. $\omega = 1$ with the current nondimensionalization.

Does or choice of ω work? Yes, figure 2 (dashed lines) indicates that the general shape is similar and the amplitude hysteresis is captured when using the parameters in table 1. But there is a problem, the amplitudes and phase difference don't match the numerical results. How can this be fixed? The answer makes the next section much simpler and makes the solution even more general: Make the total damping in equation 3 a constant.

By fixing the value of total damping to when shedding frequency equals the natural structural frequency, i.e. $\omega_q = 1$, the approximation improves. The solid line in figure 2 shows that the constant damping causes a slight mismatch between numerical results and prediction for the phase difference but that structural and wake amplitudes match. Setting the shedding frequency in the total damping to one is rather arbitrary but nonetheless works well unless μ is very low.

Before moving to the next section, let's summarize some sub-conclusions. 1) Frequency dependent damping is not well represented in the approximation, 2) forcing frequency is best set to the structural natural frequency and 3) the approximation produces three closed-

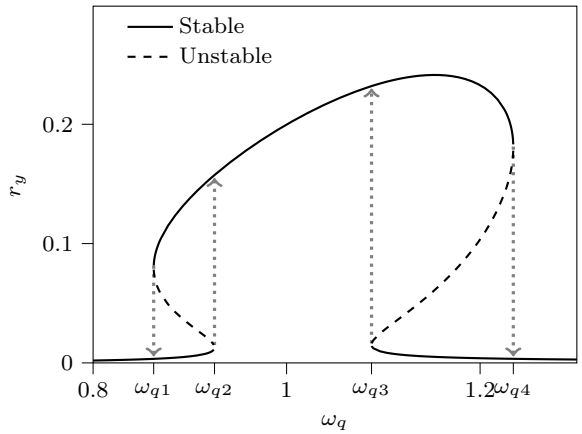

Fig. 3 Stability and boundaries of synchronization for given parameters. Dotted lines with arrows mark the jumps when sweeping ω_q.

form expressions for phase difference and amplitudes. In the next sections, an analytic closed-form solution for the synchronization regions is defined, a process that's simplified by making the total damping constant.

3 When does synchronization occur?

3.1 Existing definition

For comparison, our definition will be compared with the one found by de Langre. As mentioned, the region is found by setting D and ϵ in the equations of motion to zero. This simplifies the equations andeliminates all nonlinearities. Using traditional couple-mode flutter techniques, the synchronization region is found to be between $\omega_q = (1 \pm \sqrt{AM})^{-1}$ assuming $AM < 1$ [9]. For vortex-induced vibrations, M tends to be small making this assumption true in most cases.

3.2 Definition of synchronization

Before determining a mathematical expression for the regions for absolute synchronization (independent of time history) and conditional or hysteresis synchronization, let's focus on figure 3. The graph shows a focused view of the structural amplitude and which phase difference solutions that are stable (solid line) and unstable (dashed lines). Stability is determined by taking the derivative of equation 13 (phase difference equation) with respect to θ. A positive derivative at a given wake frequency and phase difference combination gives an unstable solution.

You might be asking yourself: Does the stable and unstable solutions correspond to a specific analytic solution of equation 13? And they do. The low amplitude solution corresponds to one specific root, high amplitude to another and the unstable to the third. Here is a new question: Can this define the synchronization region? Figure 3 shows that distinct one-way jumps between the solutions can occur between ω_{q1} and ω_{q2} and between ω_{q3} and ω_{q4}; the specific direction and location is marked by the dotted, grey arrows. These regions correspond with unstable solutions and the preceding amplitude decides future amplitudes when sweeping ω_q. This is the cause of our amplitude hysteresis.

We now have a description of when synchronization can occur but are missing a mathematical definition. Visually determining synchronization is a stepping stone to defining an an equation for the synchronization regions as a function of ω_q. This is the focus of the next section.

3.3 The synchronization region defined

The mathematical definition of synchronization is related to when unstable solutions occur, but not defined by it; two unstable regions exists with the parameters in table 1, but the regions can be negligible for other values of μ. A more rigorous definition, is when the cubic solutions giving real-only solutions change. This depends on the discriminant of equation 14.

As a refresher, three distinct real roots exists if the discriminant is positive and one real roots plus two complex conjugate roots solutions if negative. The discriminant of a cubic equation is given as $\Delta = 18abcd - 4b^3d + b^2c^2 - 4ac^3 - 27a^2d^2$ and the values of a–d are given in equations 15–18. Setting Δ to zero gives the advent or departure of the three solution regime. Here we would like to remind the reader of the benefit of constant damping: It simplifies the discriminant and the resulting polynomial equation in terms of the wake frequency.

By setting the discriminant to zero, a bi-sextic equation in terms of ω_q emerges; a sextic equation can have up to two more solutions than needed. Luckily, two of the solutions are trivial solutions are found and can be ignored: $\omega^2_{q5,6} = (D^2 + 1)/(1 - AM)$. The remaining quartic equation has the common denominator $(1 - AM)^2$ and can be eliminated. The start and end of the synchronization regions are found by solving the bi-quartic equation

$$
\begin{aligned}
0 &= c_8\omega_q^8 + c_6\omega_q^6 + c_4\omega_q^4 c_2\omega_q^2 + c_0 \\
c_8 &= (1 - AM)^2[A^2M^2 - 4D^2(1 - AM)], \\
c_6 &= 2[D^2(1 - AM)(A^2M^2 + 8) + \\
&\qquad A^2M^2(AM + 1)], \\
c_4 &= A^2M^2(D^2 - 1)^2(D^2 + 1)^2 -
\end{aligned}
$$

$$4AMD^2(5D^2+1) - 8D^2(D^2+3),$$
$$c_2 = 8D^2(AM+2)(D^2+1),$$
$$c_0 = -4D^2(D^2+1)^2, \qquad (19)$$

where only the positive solutions are kept. The solutions of equation 19 are identical to the locations marked ω_{q1}–ω_{q4} in figure 3. An analytic solution to the quartic root exists. Due to the increase in complexity and number of terms, the analytic solutions to the quartic expression are not presented.

Next, let's examine how the synchronization regions changes with the effect of mass-ratio μ, forcing strength M and damping ratio ζ. We'll also compare our solution with the one of de Langre.

4 The synchronization regions

4.1 The effect of-mass ratio

As a reminder, the force experienced by the structure inversely is proportional to the mass-ratio μ and the total damping is inversely proportional to the mass-ratio plus a constant term. This mass-ratio can be viewed as a density ratio. Viewing it as a density-ratio helps give an intuitive understanding of when high and low ratio occurs; mass-ratios is low when fluid density is high or structural mass low (e.g. in water) and the converse gives high values (e.g. in air).

Figure 4 highlights the effect of mass-ratio on the synchronization regions. For clarity, it is separated into three graphs separated by the extent of synchronization. The top graph shows the synchronization regions for very low mass-ratios, the middle for intermediate values and the bottom for very high mass-ratios. The areas filled with vertical lines marks regions of absolute synchronization and the filled grey areas conditional or hysteresis synchronization. All three plots illustrate interesting behaviors.

First, let's focus on the very low mass-ratio cases. As the mass-ratio approaches zero, the synchronization region extends from $\omega_q \approx 0.75$ to infinity. The infinite range is concurrent with the phase difference asymptotically approaching $3\pi/4$. This is not a numerical quirk and is experimentally observed by Govardhan and Williamson for vortex-induced vibrations [8]. As we increase the mass-ratio, the absolute synchronization region monotonically shrinks. The upper limit rapidly reduces at very low mass-ratios ($\mu < 10$) and changes with a rate similar to the lower limit at higher ratios.

At low mass ratios, the conditional synchronization ranges increases as the absolute synchronization region

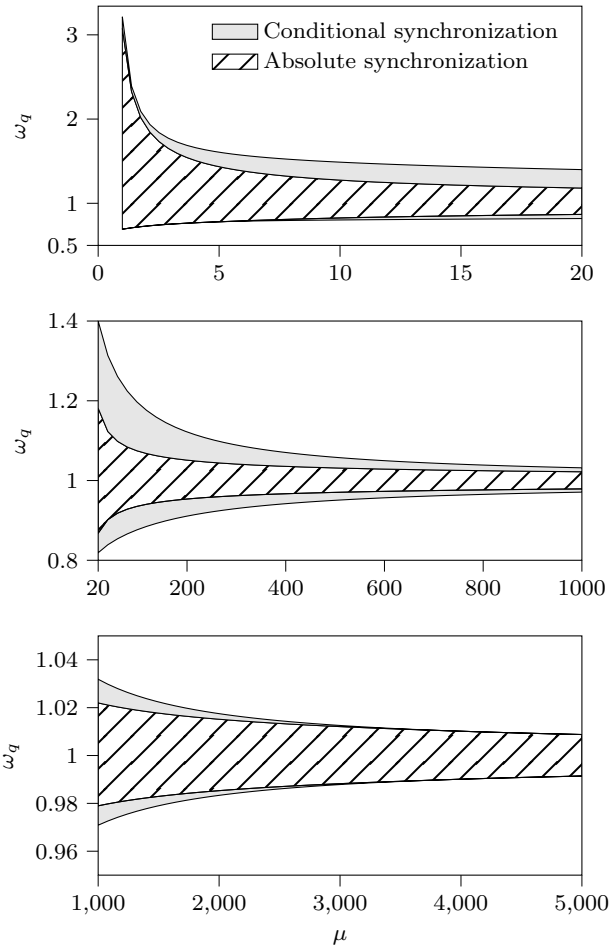

Fig. 4 Synchronization regions as a function of μ for a case with low structural damping (parameters in table 1). Three different scales of μ are plotted from top to bottom.

shrinks. At $\mu = 20$, the upper conditional synchronization range is almost as large as the absolute range indicating strong hysteresis. The lower conditional range grows with mass-ratio, but is comparatively small.

The growth ends in the intermediate region. Just like the absolute region, the upper conditional synchronization region shrinks monotonically at intermediate and high mass-ratios. The lower synchronization region follows a different path; it continues to grow until a mass-ratio near 100. At higher ratios, the lower synchronization region shrinks and approaches the extent of the upper conditional region as μ increases; this is near $\mu > 500$.

As μ increases to very large numbers, the synchronization region approaches $1 \pm \delta$ with δ being a small number that approach 0 as μ goes to infinity. This corresponds to the forcing strength and aerodynamic damping on the structural approaching zero and makes sense. No structural force means no motion. No motion means

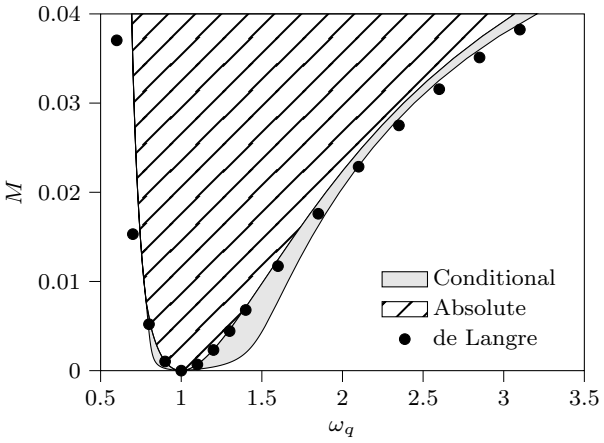

Fig. 5 "V-shaped" synchronization region and comparison of our definition with that of de Langre at selected forcing strengths/fluid speeds.

no forcing of the wake. And lack of forcing leads to two uncorrelated equations that cannot synchronize.

4.2 A different perspective and comparison with an existing definition

Traditionally, the synchronization region for a forced van der Pol oscillator is illustrated using a 2D contour plot with forcing strength as the vertical axis and forcing frequency as the horizontal. A rendition of this using our synchronization definition, with mass-scaled force, M, as the vertical axis and wake frequency, ω_q, as the horizontal, is shown in figure 5. The total damping, D, is inferred from M by keeping the forcing F constant, i.e. at constant aerodynamic conditions. This figure provides different view than figure 4 but shows the same development. The difference is that the higher mass-ratios ($\mu > 20$) are at low forcing strengths ($M < 0.002$).

Our synchronization region differs from the forced van der Pol V-shaped region by a) not being symmetric and b) having a more rounded shape. In the V-shaped graph, the lower hysteresis region becomes negligible when the mass-scaled force is more than 0.005. Even at lower values of M, the lower region tends to be insignificant when compared to both the upper conditional region and the absolute region. The upper hysteresis region is significant for most forcing strengths and its range's behavior is interesting: It first increases from $M = 0$ to $M \approx 0.0025$, then it decreases until $M \approx 0.0275$ where it again increases. The evolution of the upper solutions indicate a nonlinear behavior int heir derivative with respect to M.

It is easy to see differences when comparing our solution to that of de Langre, but there are also similarities. de Langre's synchronization region match our absolute synchronization region when $M < 0.01$ and the general development of the solutions are similar for all values of M. The solutions stop matching our absolute region when $M > 0.01$; de Langre's synchronization region starts by being wider than our absolute region and ends up even wider than the combined absolute and conditional region. Based on our result, including linear and nonlinear damping terms is more destabilizing at low values of M and more stabilizing at high. A reason for de Langre's increased synchronization region might be due to a failure of the damping simplification once M increases past 0.15; this limit is for the lowly damped structure used here.

We have now derived an expression for the synchronization regions, explored how it changes with forcing strength and compared it with an existing definition. An important parameter in vortex-induced vibrations, is the damping ratio of the structure. Therefore, the effect of mass independent dissipation in the linear equation will be studied in the next subsection.

4.3 Effect of linear dissipation

The total linear damping D contains two components where only one is directly dependent on μ. ζ's effect on the synchronization regions is investigated at three forcing strengths ($M \in \{0.0015, 0.0035, 0.0075\}$) and $\zeta \in [0, 0.02]$. In effect, we are adding a third dimension to figure 5.

Figure 6 shows this. The first thing one might notice, is that while the absolute synchronization region increases with forcing strength, the effect of ζ in the tested range is small. It is easier to see the changes in the region when comparing it with the solution of de Langre. Two thing can be noted. Firstly, the difference between de Langre's synchronization region and our absolute increase with both forcing strength and structural damping ratio. Secondly, the absolute region shrinks faster with increasing ζ when ω_{q1} merges with ω_{q2}. I.e. damping has a greater effect on the absolute synchronization region when hysteresis disappears.

The conditional regions shows an interesting behavior. As ζ increases, both conditional synchronization regions disappears (size converges to zero). There is differences between the two conditional regions. The extent of lower region decreases similarly with ζ for all three values of M. As M increases, the extent of the lower conditional synchronization region decreases in terms of both ω_q and ζ; this is not true for the upper. As M increases, the upper conditional synchronization region decreases slower with ζ and hysteresis is sustained at ζ above 0.02. The region is wider at low values of ζ and M, but can exist at higher values of ζ when forcing is

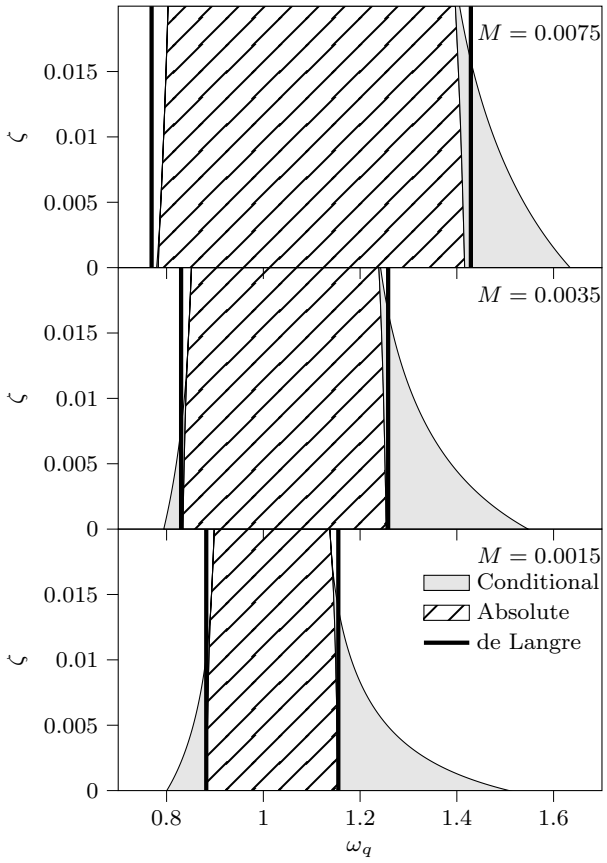

Fig. 6 Synchronization as a function of mass-independent structural dissipation.

increased. In other words, higher forcing strengths can sustain self-induced motion at higher damping levels.

The effect of mass-ratio, forcing strength and linear damping on the synchronization regions has been investigated. Before concluding and, let's discuss potential uses of our results and the usefulness.

5 Discussion

The first elephant to address is "how useful is knowing the synchronization regions?". From a structural design perspective, there are two considerations: maximum response and number of cycles. Using the approximations, response as a function of fluid speed and the number of cycles can be calculated for a given yearly speed distribution. The number of high amplitude oscillations is found by finding the total time in the synchronization region, i.e. the integral of the probability density describing time spent at a particular speed between the start and end of synchronization. For a conservative estimate, this would be between ω_1 and ω_4. For energy production, similar calculation can be made to calculate estimates of yearly production capability and peak energy production. In other words, numerical simulations to estimate the total and maximum impact can be avoided in early parts of the design process. The new estimates is also an improvement to using the previously defined synchronization region.

Amplitude hysteresis is observable for some structures experiencing vortex-induced vibration. Knowing and dealing with this can be what separates a good design from a bad. We've mentioned conservative estimates of the number of oscillations but these numbers can be improved if we know where we can have multiple solutions. When using natural flows, it is not unrealistic that there are jumps in flow speed; these jumps can lead to amplitude jumps. If we know where the jumps occur a priori, we can install devices to dissipate energy and prevent amplitude jumps in civil structures or devices that kick-start motion when producing energy.

In section 2.3, the inability to model frequency dependent damping was mentioned. Our damping approximation seems valid when $\mu > 20$ for low structural damping. When the mass-ratio is lower, the structural forcing tends to be very strong and the underlying assumptions of the nonlinear approximation are wrong; we start losing the weak nonlinearity and move towards strong nonlinearity as μ reduces closer to one. The neef for a structural damping approximation also shows a drawback with using the method of averaging. Just like how it doesn't capture quadratic nonlinearities, it seem to not capture the frequency dependent total damping given in equation 3. Using the method of averaging and a simplified damping worked well here in defining a synchronization region definition. For similar problems where the frequency dependent damping is needed, a different method of approximation (like the method of multiple scales) could be better.

As the couplings are linear, equations 1 and 2 can be rewritten in terms of y only and be reduced to one equation. This leads to a fourth order nonlinear differential equation. In addition to being able rewrite our system in terms of y we can make another statement: It is not the van der Pol equation that is conditionally forced, it is the linear structural equation. q is an intermediate fluid variable and doesn't describe the fluid dynamics but rather the overall effect of the forcing.

6 Conclusion

We have developed an expression describing the synchronization regions for vortex-induced vibration. It is also a general solution for van der Pol oscillators freely forced by a linear oscillator. The regions are determined by solving a quartic equation where the variable is the incoming fluid speed or linear van der Pol frequency.

An important step in approximating the frequency response and determining synchronization, is to find an appropriate form for structural damping; frequency dependent damping is poorly represented by the method of averaging. Simplifying the damping to a constant damping improves the prediction when compared to numerical simulations and enables us to find analytic closed form solutions for the synchronization regions.

Our synchronization definition gives better defined regions than the existing definition as it gives both the regions of absolute and conditional (hysteresis) synchronization. As shown, the size of the conditional synchronization regions initially grows as mass-ratio increases and forcing strength decreases before shrinking towards nothing. The absolute synchronization range develop slightly differently, it monotonically decreases. All synchronization regions decrease when increasing structural damping and most prominently for conditional regions. We believe the defined synchronization regions can be a great tool for prediction when vortex-induced vibrations occurs and synchronization for systems modeled using a van der Pol oscillator similarly coupled to a linear oscillator.

Acknowledgements We would like to acknowledge the help of E. Boujo in helping us find the resources needed to translate our analytic knowledge of averaging techniques to multiple degrees of freedom. The first author would like to thank the CSTB for their financial support.

Conflict of interest

The authors declare that they have no conflict of interest.

References

1. Balanov, A., Janson, N., Postnov, D., Sosnovtseva, O.: Synchronization: From Simple to Complex. Springer Series in Synergetics. Springer, Berlin (2009)
2. Barrero-Gil, A., Pindado, S., Avila, S.: Extracting energy from Vortex-Induced Vibrations: A parametric study. Appl Math Model **36**(7), 3153–3160 (2012). DOI 10.1016/j.apm.2011.09.085
3. Birkhoff, G., Zarantonello, E.H.: Jets, Wakes, and Cavities. Elsevier (2012)
4. Bishop, R.E.D., Hassan, A.Y., Saunders, O.A.: The lift and drag forces on a circular cylinder oscillating in a flowing fluid. P Roy Soc A-Math Phy **277**(1368), 51–75 (1964). DOI 10.1098/rspa.1964.0005
5. Dai, H.L., Abdelkefi, A., Wang, L.: Piezoelectric energy harvesting from concurrent vortex-induced vibrations and base excitations. Nonlinear Dyn **77**(3), 967–981 (2014). DOI 10.1007/s11071-014-1355-8
6. Facchinetti, M.L., de Langre, E., Biolley, F.: Coupling of structure and wake oscillators in vortex-induced vibrations. J Fluids Struct **19**(2), 123 – 140 (2004). DOI 10.1016/j.jfluidstructs.2003.12.004
7. Fotsin, H., Bowong, S.: Adaptive control and synchronization of chaotic systems consisting of Van der Pol oscillators coupled to linear oscillators. Chaos Soliton Fract **27**(3), 822–835 (2006). DOI 10.1016/j.chaos.2005.04.055
8. Govardhan, R., Williamson, C.H.K.: Modes of vortex formation and frequency response of a freely vibrating cylinder. J Fluid Mech **420**, 85–130 (2000). DOI 10.1017/S0022112000001233
9. de Langre, E.: Frequency lock-in is caused by coupled-mode flutter. J Fluids Struct **22**(6-7), 783–791 (2006). DOI 10.1016/j.jfluidstructs.2006.04.008
10. Meliga, P., Chomaz, J.M.: An asymptotic expansion for the vortex-induced vibrations of a circular cylinder. J Fluid Mech **671**, 137–167 (2011). DOI 10.1017/s0022112010005550
11. Skop, R.A., Griffin, O.M.: A model for the vortex-excited resonant response of bluff cylinders. J Sound Vib **27**(2), 225–233 (1973). DOI 10.1016/0022-460X(73)90063-1
12. Tamura, Y., Matsui, G.: Wake-oscillator model of vortex-induced oscillation of circular cylinder. In: Preceedings of the 5th International Conference on Wind Engineering, Vol. 2 (1979)
13. Xia, Y., Michelin, S., Doar, O.: Fluid-Solid-Electric Lock-In of Energy-Harvesting Piezoelectric Flags. Phys Rev Appl **3**(1) (2015). DOI 10.1103/physrevapplied.3.014009
14. Zhang, W., Li, X., Ye, Z., Jiang, Y.: Mechanism of frequency lock-in in vortex-induced vibrations at low Reynolds numbers. J Fluid Mech **783**, 72–102 (2015). DOI 10.1017/jfm.2015.548